In vivo determination of local skin optical properties and photon path length by use of spatially resolved diffuse reflectance with applications in laser Doppler flowmetry

Larsson, M., Nilsson, H. & Strömberg, T.

Larsson, M., Nilsson, H. & Strömberg, T., In vivo determination of local skin optical properties and photon path length by use of spatially resolved diffuse reflectance with applications in laser Doppler flowmetry, 2003, Applied Optics, (42), 7-8, 124-134. http://dx.doi.org/10.1364/AO.42.000124.

In vivo determination of local skin optical properties and photon path length by use of spatially resolved diffuse reflectance with applications in laser Doppler flowmetry

Marcus Larsson[a], Henrik Nilsson[b], Tomas Strömberg

Abstract

Methods for local photon pathlength and optical properties estimation, based on measured and simulated diffuse reflectance within 2mm from the light source, are proposed and evaluated in vivo on Caucasian human skin. The accuracy of the methods was good (2-7%) for pathlength and reduced scattering but poor for absorption estimation. Reduced scattering and absorption were systematically lower in the fingertip than in the forearm skin (633 nm). A maximum intra-site and inter-individual variation of ~35% in the average photon pathlength was found. The methodology was applied in laser Doppler flowmetry (LDF), where pathlength normalization of the estimated perfusion removed the optical property dependency.

OCIS codes: 000.4430, 160.4760, 170.3340, 170.3660, 290.7050

1. Introduction

The interaction of light with tissue is wavelength dependent, and encompasses both scattering and absorption of photons.[1,2] The scattering properties of tissue are determined by the arrangement of its structural components, and are often described by the tissue refractive index, n, the probabilistic scattering coefficient, μ_s, and the average cosine, $\langle \cos\theta \rangle$, of the angles between the incident and scattered photons, also referred to as the anisotropy factor, g. Tissue absorption is determined by its content of chromophores, e.g. hemoglobin, melanin and water, and is usually described by the absorption coefficient, μ_a. Hence, knowledge of tissue optical properties will aid in describing both chemical composition and structural arrangement of tissue. Both of these parameters are markers of tissue pathology, and could be used e.g. for detection of areas of neoplasia.[3,4]

Many authors have described methods for determining optical properties *in vivo*, usually at source detector separations, ρ, exceeding 1-2 mm, thereby losing some information about tissue structure, since the directional scattering of the photons has been randomized.[1,4-12] In addition, the resolution of the method will inevitably be reduced with greater sampling volumes, associated with increasing source detector distances.

Laser Doppler flowmetry (LDF) is a well-established method for monitoring microvascular perfusion *in vivo*.[13-17] The LDF output signal is generated from the interaction between photons and moving scatterers, mainly red blood cells (RBCs). The

[a] corresponding author, [b] co-first author
Department of Biomedical Engineering, Linköping University, S-581 85 Linköping, Sweden
E-mail to corresponding author: marla@imt.liu.se

LDF perfusion estimate is affected both by the concentration and the velocity of the moving scatterers.[18] Further, it has been shown that the perfusion estimate is proportional to the migrated photon pathlength (pl), at a constant concentration and velocity of the moving scatterers.[16,19,20] Detected photons migrate different distances through tissue, i.e. have different pathlengths, depending on the source detector separation, and the optical properties. This is easily understood, since the inverse of the sum of μ_s and μ_a, also called the mean free path (mfp), describes the average distance between events of photon tissue interaction. Therefore, it is expected that the influence of variations in optical properties on the LDF signal[21] could be dramatically reduced, if the pathlength could be estimated locally. This would allow inter- and intraindividual comparisons of LDF measurements. In a previous study, we have presented a method that can predict the photon pathlength, at source detector separations up to two millimeters, with a root mean square (rms) error of about five per cent.[19]

The aim of this study is to propose a method that minimizes the influence of optical properties on the LDF perfusion estimate. The method was evaluated in 11 human subjects, *in vivo*, and the inter- and intraindividual LDF perfusion variations, related to changing optical properties, were estimated. In addition, local variations in optical properties and pathlength were assessed *in vivo*, at different human skin sites.

2. Materials and Methods

A. Simulation Setup

The diffuse reflectance was studied at small source detector separations (up to 1.61 mm), for optical properties relevant to human skin. The diffusion approximation of the transport equation is not generally applicable if $\rho\mu_s' < 10$, or for small source detector separations up to 2 mm.[5,22] Furthermore, the diffusion approximation is only valid when $\mu_a << \mu_s'$.[23] Therefore, photon migration was modeled by means of Monte Carlo simulations (MontCarl 2001, version 20.01 a).[24]

The simulation setup consisted of a homogenous semi-infinite slab (infinite in the x- and y-dimensions), with a thickness of 100 mm (z dimension). A low concentration of moving scatterers, corresponding to $\mu_s = 0.1\ \text{mm}^{-1}$, with a constant velocity, v = 1.0 mm/s, parallel to the slab surface, was introduced in the model. All scattering events were modeled with a modified Henyey-Greenstein phase function,[25]

$$p(\theta) = \frac{1}{4\pi}\left[\beta + (1-\beta)\frac{1-g_{HG}^2}{(1+g_{HG}^2 - 2g_{HG}\cos\theta)^{3/2}}\right] \quad (1)$$

where $\beta = 0.04$ ($\beta = 0$ for the simulations of tissue phantom A and B, see below) describes the isotropic component of the phase function. θ is the deflection angle and g_{HG} the anisotropy factor. This combination of one isotropic, and one highly forward scattering component has been found to adequately describe photon migration through biological tissues.[4,5] Doppler shifts, due to photon interaction with moving scatterers, were stored for estimation of the LDF perfusion. The refractive index of the slab was set to n = 1.44, which is considered relevant for human skin at 632.8 nm,[26,27] whereas it was

set to $n = 1.0$ for the ambient air. A divergent beam, with a rectangular intensity distribution, was setup to create a circular injection area (0.1 mm in radius), located at the center of the slab surface. All photons exiting the upper slab surface at a radial distance (ρ) from the center of the source in the range $0.13 \leq \rho \leq 1.71$ mm were detected, and transformed mathematically into a linear array of fibers, identical to the LDF probe used in the present study.[21] In all simulations, 10^6 photons were detected, and subsequently normalized by the number of emitted photons. A similar arrangement has previously been used by authors when developing an algorithm for prediction of photon pathlength at source detector separations up to two mm.[19]

Four sets with different combinations of optical properties were defined (Table 1) and simulated. Set one (main reference set) and two (main validation set) encompassed a large range of optical properties, considered relevant for human skin at $\lambda = 632.8$ nm, both based on the literature,[2,26-28] and preliminary *in vivo* results. Set three (sub reference set) and four (sub validation set) were both sub-sets of set one and two, respectively, with equal μ_s' and $\langle\cos\theta\rangle$, but a much more narrow range of μ_a. Preliminary *in vivo* results indicated that this narrower range of μ_a corresponds to the bulk of the predicted values in human forearm skin. The optical properties of set one through four were spaced equidistantly, μ_a and μ_s' in a logarithmic sense, and $\langle\cos\theta\rangle$ in a linear sense. In addition, two more combinations of optical properties (Table 1), denoted set five (tissue phantom A) and six (tissue phantom B), were defined and simulated in order to mimic two tissue phantoms with known optical properties. For each set of optical properties all possible combinations of μ_a, μ_s' and $\langle\cos\theta\rangle$ were simulated, resulting in a total of 6x5x3 + 5x4x2 + 5x5x3 + 4x4x2 + 1 + 1 = 239 simulations (Table 1).

Table 1. Simulated optical properties. Set 1-4 corresponds to main reference, main validation, sub reference and sub validation set, respectively. Set 5 corresponds to tissue phantom A, and set 6 to tissue phantom B. Within each set all possible combinations of μ_a, μ_s' and $\langle\cos\theta\rangle$ were simulated, resulting in a total of 239 simulations.

Set	μ_a (mm^{-1})	μ_s' (mm^{-1})	$\langle\cos\theta\rangle$
1	[0.001, 0.003, 0.01, 0.03, 0.1, 0.3]	[0.8, 1.2, 1.8, 2.7, 4.05]	[0.8,0.85,0.9]
2	[0.002, 0.006, 0.02, 0.06, 0.2]	[1, 1.5, 2.25, 3.375]	[0.825, 0.875]
3	[0.0075, 0.015, 0.03, 0.06, 0.12]	[0.8, 1.2, 1.8, 2.7, 4.05]	[0.8,0.85,0.9]
4	[0.01, 0.02, 0.04, 0.08]	[1, 1.5, 2.25, 3.375]	[0.825, 0.875]
5	0.0405	2.738	0.815
6	0.0532	8.429	0.815

Out of the first four sets of simulated data, set two was used for validation of the optical properties and pathlength predictions based on set one, and similarly for set four and three. The optical properties of set two and four were chosen to maximize the linear distances to the nearest neighbors in set one and three, respectively.

B. Measurement Setup

Measurements were carried out using a digital multi channel laser Doppler flowmetry (LDF) probe system (Figure 1).[21] The probe consisted of eight multi-mode step index fibers (NA = 0.37) aligned in a row, each with a diameter of 230 µm (including 30 µm cladding), and with center-to-center separations of 230 µm. Light was delivered by a He-

Ne laser at 632.8 nm, through one emitting fiber (fiber number zero). The sixth fiber from the emitting one displayed a reduced light transmission, and hence, counting from the emitting one, fibers number one to five and seven were used for receiving backscattered light.

The light intensity from each of the six receiving fibers was detected by two photodetectors. By adding the two photocurrents, the magnitude of the reflectance, R_i, was found. In order to reduce the common mode noise, the AC_i, or time varying part, of the raw LDF signal was determined as the difference of the two photocurrents.[29] Further, the AC_i signal was amplified and band pass filtered with a third order Butterworth filter between 20 Hz and 12.5 kHz, eliminating low-frequency distortions (tissue motions) as well as high frequency signals that mainly consists of noise generated by the photodetector.

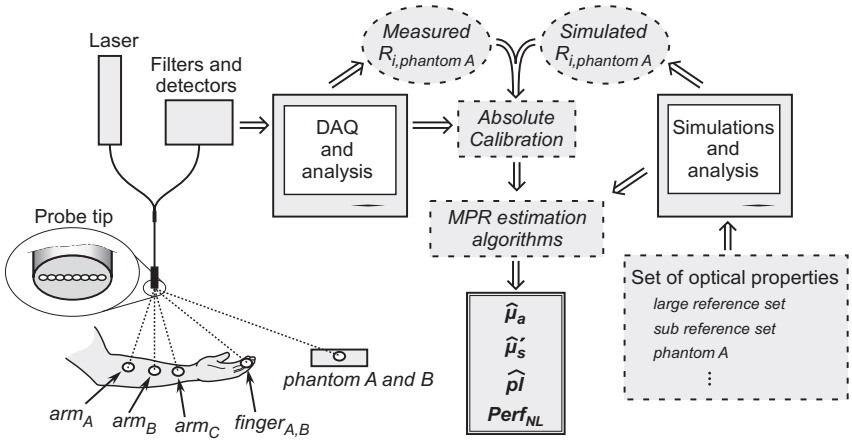

Figure 1. Experimental set-up and data analysis flow chart, illustrating the data acquisition system (DAQ), measurement-simulation calibration (R_i: reflected intensity), estimation algorithm (MPR: multiple polynomial regression) and the resulting output ($\hat{\mu}_a$: estimated absorption coefficient; $\hat{\mu}_s'$: estimated scattering coefficient; $\hat{pl}$: estimated photon pathlength; $Perf_{NL}$: normalized and linearized LDF perfusion).

The preprocessed AC_i and R_i signals were sampled with a 12-bit data acquisition card at 50 kHz (DAQPad-6070E, National Instruments Corporation), using a range of ±10 Volts. Data acquisition software was developed in LabVIEW 6.0 (National Instruments Corporation), and analysis software in MATLAB® 6.0. Each measurement was carried out over 10 seconds.

In vivo measurements were carried out over two days in eleven Caucasian human subjects, out of which five were women. One person had a slightly darker skin complexion, than the other ten. Written informed consent was obtained from all subjects, prior to the measurements. The laser was turned on at least 120 minutes prior to the first measurement, and the fiber tip was wiped off with alcohol between measurements on the different sites. The ambient air temperature was kept within a narrow range around

22.0°C, and the output power of the laser was checked regularly, and found to be approximately 1.2 mW.

Both days, a calibration protocol was carried out, before commencing the measurements on the subjects. This protocol included measurements on two tissue phantoms (A and B) with known optical properties (with corresponding optical properties as in set five and six in Table 1). A short description of how the optical properties were determined has been presented by Larsson *et al*.[21] The stability of the system was verified both by the measurements on the tissue phantoms, and by measurements on a piece of polyacetal plastic (Delrin®). The AC_i noise level was determined as a function of R_i, by measurements at various distances between the probe and the piece of Delrin®. Calibration measurements were also carried out in the PF 1001 motility standard solution (Perimed AB, Stockholm), with the laser connected to one fiber at a time, and light collected two fibers away. This procedure ensured a constant emitting-receiving fiber separation and thus a constant photon pathlength for all receiving fibers, resulting in one AC_i gain factor for each LDF channel. These gain factors were used to remove any differences in the AC-amplification of the various LDF channels.

The subjects were sitting down comfortably during the measurements, and rested approximately 15 minutes prior to the first measurement. Measurements were made on two naevi ($naevus_{A\text{-}on}$ and $naevus_{B\text{-}on}$), either on a forearm, leg or the back, with the fiber inserted in a probe holder that was attached to the skin with a double adhesive tape. The naevi were inspected and their sizes measured by a medical doctor. Some naevi were very small (about 2 mm), and it was therefore difficult to ensure probing of the relevant area. Since it was uncertain in these cases if the actual naevus, or adjacent skin, had been probed, they were not considered in the statistical analysis. Five measurements were made on each site, with the probe being lifted, and reinserted into the holder between each measurement. The probe was designed to ensure the same location of the probe in the holder each time, both rotational- and depth-wise. Five measurements were made adjacent to each one of the naevi ($naevus_{A\text{-}off}$ and $naevus_{B\text{-}off}$), using the same probe holder. Furthermore, five measurements were made on the volar aspect of the proximal forearm, using the probe holder (arm_A), and five measurements were made as a stepwise scan, with 1 mm steps, on two different skin sites distal to the first one (arm_B and arm_C), using a computer controlled robot with a standardized mild pressure (Desensor, Cenova AB, Sweden). Finally, a similar stepwise scan was performed on the volar aspect of the pulp of digits III and IV ($finger_A$ and $finger_B$, respectively). In all measurements, macroscopically visible superficial blood vessels, hair and pigmentation variations, were avoided as far as possible.

C. Analysis of Simulated Data

The simulated data was preprocessed in accordance with previous studies, transforming the detector surface into a linear array of detecting fibers.[19,21] This resulted in simulated LDF power spectrum (P_i), LDF perfusion ($Perf_i$), reflectance (R_i), and average pathlength (pl_i). The pl_i is in this context defined as the average of the distances migrated by the photons from point of entry (source fiber) to point of detection (ith detector fiber). The concentration of moving blood cells ($CMBC_i$) estimate was calculated according to

Equation 2. The linearized perfusion, $Perf_{Li}$, was determined using a method described by Nilsson.[18]

$$CMBC_i = \frac{\sum_{\omega} P_i(\omega)}{R_i^2} \tag{2}$$

$$H_i = \frac{CMBC_i}{CMBC_{i,motility}} \quad ; H_i \in [0,1] \tag{3}$$

$$Perf_{Li} = \left(\frac{1 - aH_i}{1 - bH_i} \right) Perf_i \tag{4}$$

where a = 0.885 and b = 0.939. $CMBC_{i,motility}$ corresponds to calibration measurements in a motility standard (PF 1001 motility standard solution, Perimed AB, Sweden). Preliminary results indicated that a minor non-linearity in $Perf_{Li}$ vs pl_i, existed at short pl_i. This was corrected for by applying Equation 5, resulting in the *adjusted average photon pathlength*, pl_i'. Finally, $Perf_{Li}$ was normalized by pl_i', yielding $Perf_{NLi}$:

$$pl_i' = pl_i + pl_i^c \tag{5}$$

$$Perf_{NLi} = \frac{Perf_{Li}}{pl_i'} \tag{6}$$

The value of c (c = 0.504) was derived by least squares fitting of data from the main reference set.

D. Analysis of measured *in vivo* data

The measured R_i profile of tissue phantom A was related to the corresponding simulated reflectance profile, by calculating the ratio between simulated and measured data. The resulting R_i calibration factors, one for each fiber, were used fore rescaling all measured R_i data prior to any analysis. Both the sampled AC_i and the calibrated R_i signals were then divided into batches of 1024 values. For each batch, the average R_i and the AC_i power spectral density (PSD_i) were calculated. The resulting PSD_i values were integrated, both with and without ω-weighting, over the frequency span up to 12.5 kHz, and normalized by R_i^2, resulting in estimations of LDF perfusion ($Perf_i$), and concentration of moving blood cells ($CMBC_i$), respectively. The $Perf_i$ and $CMBC_i$ were then both noise compensated and normalized by the individual AC_i gain factors. Finally, the $Perf_i$, $CMBC_i$ and R_i values were averaged over the ten seconds of measurement data, and the $Perf_i$ were linearized according to Equation 4. In the final analysis, only the $Perf_i$ from fibers one through five were used, because of an unsatisfactory low signal-to-noise ratio

in fiber seven. However, the R_i values from fiber seven were used in the fitting of the reflectance data to Equation 7.

E. Data Preprocessing and Estimation Methods

A logarithmic form of a modified expression originating from diffusion theory, introduced by Groenhuis *et al*[8], was fitted to the simulated and measured R_i:

$$\ln R_i = m_1' - m_2 \ln \rho_i - m_3 \rho_i \tag{7}$$

where $m_1' = \ln m_1$ and ρ_i = center-to-center separation between the source and the ith detector fiber. This logarithmic form of the expression was introduced in order to minimize the relative fitting error in a least squares sense, using linear regression, solving for m_1', m_2 and m_3. The resulting m_k-values have previously been found to accurately describe the shape and the absolute magnitude of the reflectance profile.[19] ln R_i was recalculated, using the fitted m_k-data; thus, reducing the sensitivity to potential reflectance perturbations in one or several fibers. In this study, m_k values were calculated based on the diffuse reflectance from fibers one to five and seven, counting the emitting fiber as number zero.

In a previous paper, we have described several different methods for prediction of the average pathlength.[19] We found that a multiple polynomial regression (MPR) model of the third degree, using m_1, m_2 and m_3 as predictors, resulted in the best estimations of pl_i. In the present study, we tried to further simplify the model, and analysis showed that we obtained consistent and among the most accurate and precise predictions both of the optical properties and pl_i using ln R_i, i = [3, 7] as predictors in the MPR model. The same model was used for prediction of μ_a, μ_s' and pl_i:

$$\hat{\alpha} = \hat{\alpha}(\ln R_3, \ln R_7) = \sum_{j,k} a_{jk} \ln R_3^j \ln R_7^k \ , \ \ j+k \le 3 \tag{8}$$

hence,

$$\begin{aligned} \hat{\alpha} = {} & a_{00} + a_{10}\ln R_3 + a_{01}\ln R_7 + a_{11}\ln R_3 \ln R_7 + a_{20}\ln R_3^2 + a_{02}\ln R_7^2 + \ldots \\ & \ldots + a_{12}\ln R_3 \ln R_7^2 + a_{21}\ln R_3^2 \ln R_7 + a_{30}\ln R_3^3 + a_{03}\ln R_7^3, \end{aligned} \tag{9}$$

where $\hat{\alpha}$ is the predicted data value, in this case either $\hat{\mu}_a$, $\hat{\mu}_s'$ or $\widehat{pl}_i$. For each of these three parameters, a set of polynomial coefficients (a_{jk}) where derived by fitting equation 9 to the corresponding parameter in a least square sense, using the reflectance data from either of the reference sets.

The precision and accuracy of the prediction method, described as the relative estimation error ($(\hat{\alpha} - \alpha)/\alpha$), was evaluated by applying it to the simulated data from either of the validation set; The μ_a, μ_s' and pl_i of set two were predicted using simulated data from set one (Table 1) for deriving the estimation polynomials, and similarly, the parameters of set four were predicted using set three as the reference set. The robustness of the prediction method was evaluated by multiplying all reflectance profiles with a normally

distributed noise (mean = 1, sd = 0.05), roughly corresponding to the worst-case differences seen between the simulations and measurements of the two tissue phantoms.

In addition, principal component analysis (PCA) of $\ln R_i$, evaluated at all fiber separations, was used to select the most relevant predictors for the estimation algorithm. However, the first and second principal components resulted in none or minute improvements of accuracy and precision, compared to using $\ln R_i$, $i = [3, 7]$, as predictors. For this reason, PCA was not used as part of the final analysis of the measured reflectance data.

For the purpose of increasing prediction accuracy in the *in vivo* measurements, set one and two were concatenated into one set (joined main reference set), and set three and four into one (joined sub reference set). If the normalized, preprocessed logarithmic reflectance data fell within the convex hull of the joined sub reference set, then that data was used in the prediction process. Otherwise, the joined main reference set was used for the prediction. If the logarithmic reflectance data fell outside the convex hull of the joined main reference set, it was considered an outlier, and discarded from the results.

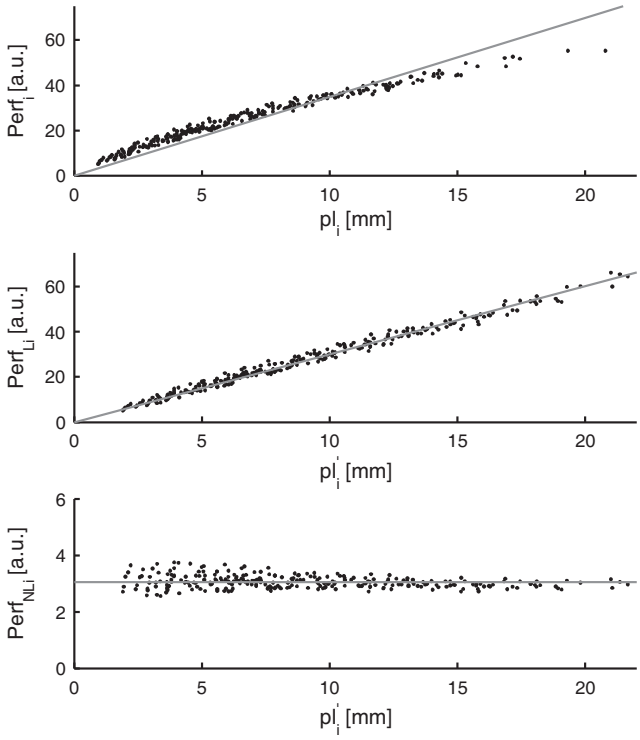

Figure 2. Relationship between; a) photon pathlength (pl_i) and perfusion ($Perf_i$), b) compensated pathlength (pl_i') and linearized perfusion ($Perf_{Li}$) and c) compensated pathlength (pl_i') and normalized and linearized perfusion ($Perf_{NLi}$). All of the presented data is based on Monte Carlo simulations with a fixed anisotropy factor ($\langle \cos\theta \rangle = 0.85$) and a range of absorption and reduced scattering coefficients (main reference set). Source detector separation, $\rho_i = 0.23, 0.46, \ldots, 2.07$ mm.

3. Results

A. Simulation and Validation

In Figure 2a, the estimated perfusion, $Perf_i$, is plotted versus average photon pathlength, pl_i, for a range of simulated optical properties (main reference set, Table 1) and source detector separations (ρ_i = 0.23, 0.46, …, 2.07 mm). The simulated perfusion exhibited a non-linear relationship with pl_i (rms of the relative error with respect to a linear fit was 29.2%). As seen in Figure 2b, $Perf_{Li}$ was virtually linear vs pl_i' (rms of the relative error with respect to the linear fit was 7.6%). $Perf_{NLi}$ was independent of pl_i', but displayed some stochastic variations for the shorter pathlengths (Figure 2c).

In Table 2, $Perf_{NLi}$ (perfusion normalized by $\widehat{pl}_i'$) is given for the main and sub validation sets. Normalization of the simulated LDF perfusion reduced the coefficient of variation (CV) of the perfusion estimate 5-6 times to ~6%, considering all source detector separations (0.23 - 1.15 mm). When perfusion estimates from only one fiber were evaluated, the CV was decreased 2-4 times to ~6%, depending on the utilized reference set. Even larger improvements were seen in the range of the perfusion values.

The proposed modified MPR prediction algorithm, applied to the simulation data (main and sub validation sets), resulted in rms values of the relative estimation errors of 2-3% for the pathlength estimations at fiber separations of 0.23 ($\widehat{pl}_1$) and 1.15 mm ($\widehat{pl}_5$), as seen in Table 3. The rms values of the relative estimation errors were increased to 6-7%, when the reflectance data was disturbed with noise.

Table 2. Variations in perfusion estimate for pathlength-normalized and linearised perfusion ($Perf_{NLi}$) and linearised perfusion ($Perf_{Li}$), expressed as CV (SD/mean) and range (min-max). *All* fibers refers to the five fiber separations ρ_i = 0.23, 0.46, …, 1.15 mm.

Main validation set with <cos θ> = 0.825			
Fiber:	All	1	5
CV($Perf_{Li}$):	0.39	0.21	0.23
CV($Perf_{NLi}$):	0.063	0.061	0.057
range($Perf_{Li}$) [a.u.]:	7.0-39.6	7.0-14.8	18.9-39.6
range($Perf_{NLi}$) [a.u.]:	3.1-4.1	3.1-3.9	3.1-3.8
Sub validation set with <cos θ> = 0.825			
Fiber:	All	1	5
CV($Perf_{Li}$):	0.34	0.13	0.13
CV($Perf_{NLi}$):	0.066	0.061	0.065
range($Perf_{Li}$) [a.u.]:	8.3-34.1	8.3-13.0	23.1-34.1
range($Perf_{NLi}$) [a.u.]:	3.0-4.2	3.2-3.9	3.0-3.8

Table 3. The rms of the relative estimation errors using the third degree MPR estimation algorithm, applied to the validation simulations of either the main and the sub reference sets, with and without 5% (rms) noise. $\widehat{pl}_1$ and $\widehat{pl}_5$ refer to pathlength estimations for a fiber separation of 0.23 and 1.15 mm, respectively.

Evaluation simulation	Noise (%)	$\hat{\mu}_a$	$\hat{\mu}_s'$	$\widehat{pl}_1$	$\widehat{pl}_5$
Main validation set	0	0.30	0.028	0.032	0.031
Main validation set	5	0.51	0.073	0.061	0.065
Sub validation set	0	0.11	0.019	0.024	0.030
Sub validation set	5	0.29	0.065	0.055	0.071

The MPR algorithm used for estimation of pl_i, was also applied to estimate the absorption and reduced scattering coefficients. Evaluating the precision of this prediction algorithm for simulated data yielded an rms of the relative estimation error of 2.8% for $\hat{\mu}_s'$ and 30% for $\hat{\mu}_a$, using the main validation set (Table 3). Corresponding rms errors for the sub validation set were 1.9% and 11%, respectively. The noise disturbed reflectance data resulted in a decreased precision in both $\hat{\mu}_s'$ and $\hat{\mu}_a$, displaying an rms of the relative estimation error of 7.3% and 51%, respectively, for the main validation set. Analogous rms errors for the sub validation set were 6.5% and 29%, respectively. Furthermore, the precision of the developed method was verified by measurements on the tissue phantoms. Using tissue phantom B for calibration, resulted in a $\hat{\mu}_a$ over-estimation of 15% and $\hat{\mu}_s'$ under estimation of 12% for the measurements on tissue phantom A. This could be compared to an over-estimation of $\hat{\mu}_a$ of 9.4% and an under estimation of $\hat{\mu}_s'$ of 5.5%, when applying the prediction algorithm to the reflectance profiles derived from simulations of tissue phantom A.

B. In vivo Measurements

An example of *in vivo* pathlength estimations is shown in Figure 3, where four different measurement locations on the skin of one individual are depicted. The figure indicates that $\widehat{pl}_i'$ not only depends on the fiber separation, but also on what skin site is being

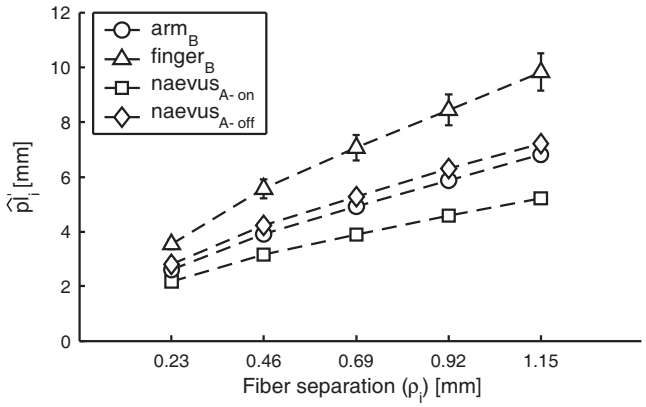

Figure 3. Predicted photon pathlength (mean ± SD) at four different skin locations in one individual for five fiber separations, ρ_i = 0.23, 0.46, …, 1.15 mm, and λ = 632.8 nm.

Table 4. *In vivo* intra-site variability of $\hat{\mu}_a$, $\hat{\mu}_s'$, $\widehat{pl}_i'$ and LDF perfusion, calculated as the average CV (SD/mean) for each site over all individuals. Measurement series with less than three acceptable estimations (data points falling inside the convex hull of the reference simulations) were excluded.

	Site		
Variable	*arm*$_A$	*arm*$_B$	*finger*$_A$
$\hat{\mu}_a$	0.064	0.21	0.50
$\hat{\mu}_s'$	0.013	0.058	0.072
$\widehat{pl}_1$	0.0088	0.030	0.044
$\widehat{pl}_5$	0.011	0.040	0.057
$Perf_{L1}$	0.15	0.22	0.29
$Perf_{L5}$	0.16	0.17	0.18
$Perf_{NL1}$	0.15	0.22	0.30
$Perf_{NL5}$	0.16	0.18	0.21
n	11	11	9

probed. The average intra-site $\widehat{pl}_i'$ variability (Table 4) for the *arm*$_B$ (CV: 3-4%) and the *finger*$_A$ (CV: 5-6%) measurements were smaller than the inter-individual variability in average $\widehat{pl}_i'$ (Table 5) for the *arm*$_B$ (CV: 7-9%; max/min: 26-36%) and the *finger*$_A$ (CV: 7-9%; max/min: 25-34%) measurements. In addition, the inter-site $\widehat{pl}_i'$ variation between the *finger*$_A$ and the *arm*$_B$ measurements were on average 29-35% (Table 6). Repeated $\widehat{pl}_i'$ measurements of the exactly same skin location (site *arm*$_A$) showed an average CV of ~1%, which is ~3-4 times less than the CV calculated from $\widehat{pl}_i'$ measurements of five different locations in an adjacent skin area (site *arm*$_B$), measured as a scan with an offset of 1 mm (Table 4).

Table 5. Mean and inter-individual variability of $<\hat{\mu}_a>$, $<\hat{\mu}_s'>$ and $<\widehat{pl}_i'>$, for different skin sites ($\lambda = 632.8$ nm). The brackets $<>$ refer to an individual average of all measurements within each site. $\widehat{pl}_1'$ and $\widehat{pl}_5'$ refer to pathlength estimations for fiber separations of 0.23 and 1.15 mm, respectively.

	Variable	$<\hat{\mu}_a>$		$<\hat{\mu}_s'>$		$<\widehat{pl}_1'>$		$<\widehat{pl}_5'>$	
Site	***n***	**mean**	**CV**	**mean**	**CV**	**mean**	**CV**	**mean**	**CV**
arm$_A$	11	0.044	0.54	2.1	0.13	3.0	0.083	8.1	0.10
arm$_B$	11	0.052	0.44	2.1	0.061	2.9	0.071	7.8	0.093
arm$_C$	11	0.043	0.36	2.2	0.089	3.0	0.052	8.1	0.070
finger$_A$	10	0.0085	0.68	1.4	0.12	3.7	0.068	10.4	0.087
finger$_B$	10	0.0056	0.69	1.4	0.096	3.8	0.052	11.7	0.065
naevus$_{A\text{-}on}$	6	0.15	0.51	1.4	0.31	2.5	0.091	6.1	0.11
naevus$_{A\text{-}off}$	6	0.036	0.52	1.8	0.073	3.1	0.072	8.3	0.11
naevus$_{B\text{-}on}$	4	0.086	0.52	1.8	0.25	2.7	0.15	7.0	0.18
naevus $_{B\text{-}off}$	4	0.040	0.64	2.0	0.14	3.1	0.11	8.3	0.14

Table 6. *In vivo* inter-site variability of $\hat{\mu}_a$, $\hat{\mu}_s'$, $\widehat{pl}_i'$ and LDF perfusion, calculated as the mean of the individual ratios $\langle finger_A \rangle / \langle arm_B \rangle$. The brackets < > refer to an individual average of all measurements within each site.

Variable	mean(<$finger_A$> / <arm_B>)
$\hat{\mu}_a$	0.18
$\hat{\mu}_s'$	0.66
$\widehat{pl}_1$	1.29
$\widehat{pl}_5$	1.35
$Perf_{L1}$	6.0
$Perf_{L5}$	5.1
$Perf_{NL1}$	4.6
$Perf_{NL5}$	3.8
n	10

A typical example of the distribution of the optical properties within one individual is presented in Figure 4. This figure clearly shows that the difference in predicted optical properties between the arm and the finger sites was greater than the variations within one location – a statement valid for all our measurements, as displayed in Table 4 and 6. In general, fingertips had lower $\hat{\mu}_a$ and $\hat{\mu}_s'$ than volar forearm skin, whereas naevi had higher $\hat{\mu}_a$ and lower $\hat{\mu}_s'$ than surrounding skin, as seen in Table 5. Repeated measurements on the exactly same skin location (site arm_A) showed an average CV of the predicted optical properties of 6.4% for $\hat{\mu}_a$ and 1.3% for $\hat{\mu}_s'$. This is ~3-4 times less than the CV calculated from $\hat{\mu}_a$ and $\hat{\mu}_s'$ estimations of five different locations in an adjacent skin area (site arm_B), measured as a scan with an offset of 1 mm (Table 4).

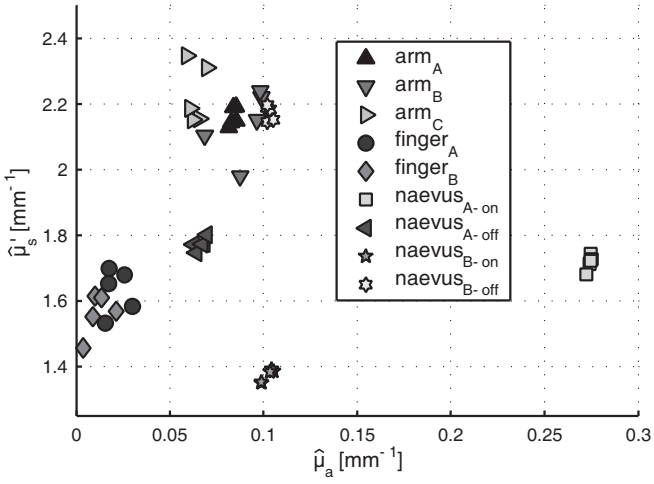

Figure 4. Absorption coefficients ($\hat{\mu}_a$) and reduced scattering coefficients ($\hat{\mu}_s'$), measured at nine different skin locations in one individual, at λ = 632.8 nm.

$Perf_{NLi}$ was in some cases independent of ρ_i *in vivo*, but more often it increased as a function of ρ_i. A typical example of this is shown in Figure 5, where $Perf_{NLi}$, measured on the volar side of the forearm, is presented for three individuals and five different emitting receiving fiber separations. No significant difference between the intra site variations of $Perf_i$ and $Perf_{NLi}$ was seen (Table 4).

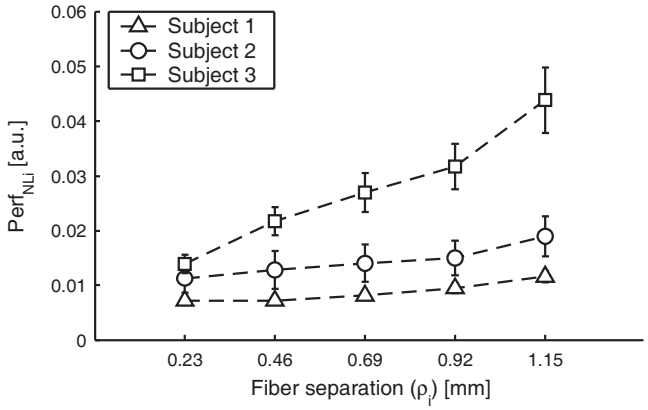

Figure 5. Calibrated, normalized and linearized perfusion ($Perf_{NLi}$; $\bar{m}\pm$sd) measured in three different individuals on the volar side of the forearm with five different fiber separations.

Out of the 495 measurements carried out in this study, a total of 37 (7%) fell outside the convex hulls of both the joined main- and joined sub-reference sets, and were thus discarded, while a total of 407 (82%) measurements fell inside the joined sub reference set. None of the volar forearm skin measurements (arm_A, arm_B or arm_C) fell outside the convex hull of the sub reference set.

4. Discussion

The origin of the LDF perfusion estimate, Perf, is found in the interaction between moving red blood cells (RBCs) and laser light. The interaction probability depends on the concentration of moving RBCs and the migrated photon pathlength. According to LDF theory,[16,20] as well as Monte Carlo simulations (Figure 2a), the relationship between average photon pathlength and LDF perfusion is not completely linear. The non-linearity in the perfusion estimate is partly caused by photons that have been Doppler shifted multiple times. Nilsson has previously described a method for linearization of the measured perfusion estimate versus the concentration of moving RBCs.[18] By applying his algorithm to the simulated data in the present study, an almost linear relationship between the perfusion estimate and the pl_i was obtained. However, there were still non-linearities at small pathlengths. These non-linearities might be explained by the fact that we use the average photon pathlength and not the actual pathlength distribution. This minor non-linearity was corrected by adjusting the photon pathlength according to Equation 5 (Figure 2b). Further, it should be noted that the perfusion estimate is strongly related to the anisotropy factor of the moving scatterers. Only results from simulations with

$\langle\cos\theta\rangle$=0.85 are presented in Figure 2. Similar linear relationships were derived with other anisotropy factors.

The established unique relationship between estimated perfusion and adjusted pathlength, clearly indicates that it is possible to minimize the pathlength dependence of $Perf_{Li}$ by normalization with pl_i' (Equation 6), resulting in $Perf_{NLi}$ (Figure 2c). The random fluctuations in $Perf_{NLi}$ vs pl_i for short pathlengths, are believed to partly originate from the fact that one million detected photons probably are not sufficient when simulating small fiber separations and low blood cell concentrations. One possible explanation is that when analyzing a LDF simulation, one not only needs information regarding the location where a reflected photon is detected, but also the size of the Doppler shift; i.e. two, in stead of one, dimensions are simulated. These fluctuations may also stem from our choice of merely considering the average photon pathlength (or pl_i') for each fiber, and not the actual pathlength distribution of the detected photons. The longer the pathlength that a photon migrates, the greater the likeliness that it suffers multiple Doppler shifts. Hence, for any given detecting fiber, the average pl_i may be constant, but the corresponding pathlength distribution may vary in such a way, that multiple Doppler shifts are more likely in one case than in the other; thus, resulting in perfusion variations that are not related to the average photon pathlength.

By pl_i'-normalizing the simulated $Perf_{Li}$, the CV of the resulting $Perf_{NLi}$ was considerably reduced, compared to $Perf_{Li}$ (Table 2). This reduction was seen both if considering individual fibers, and even more pronounced if compounding all detection fibers. In essence, this reduction in CV suggests that the derived perfusion estimate is independent of pl_i, and hence of optical properties and source detector separation, which is evident in Figure 2c. Thus, this correction might, in effect, enable us to make inter- and intra-individual comparisons of LDF perfusion recordings in various organs. With an appropriate calibration method, absolute LDF perfusion recordings would be feasible.

In applying the aforementioned normalization algorithm to measurements on tissue, it is necessary to know the average photon pathlength. We have previously described a method for estimation of the average photon pathlength based on the diffuse reflectance profile.[19] In the present study, we propose an improved and simplified estimation method, based on a third degree multiple polynomial regression (MPR) model. The proposed method was found to be accurate and precise, with an rms value of the relative estimation error of about 2-3% for the pathlength estimations, as well as robust, with rms errors of 6-7% after addition of noise (Table 3).

The pathlength estimates were site dependent, as well as almost linearly increasing with increasing source detector separation. In the specific case shown in Figure 3, the pathlength was more or less doubled on going from a naevus to a fingertip. It is known that the optical properties vary from tissue to tissue.[2,26] Indeed, the increase of the pl can be explained by the absorption coefficient, which was estimated to be about 10 times lower in the fingertip compared to the naevus (Figure 4).

The recordings on fingertip display on average 29-35 % longer $\widehat{pl}_i'$, compared to the forearm measurements (Table 6). Consequently, due to the linear relationship between $Perf_{Li}$ and $\widehat{pl}_i'$, traditional un-normalized LDF perfusion readings from fingertips would, in this case, be over-estimated by on average 29-35 %, in comparison with the

measurements on the volar aspect of the forearm, assuming a homogenous tissue perfusion. Looking at one site, e.g. volar forearm, $\widehat{pl}_i'$ varied up to ~40 % (max/min) between individuals in the present study. These results clearly show the need for pl_i' normalization when comparing LDF perfusion recordings from different individuals and/or measurement locations, even with probe separations typical for LDF.[16] This is contrary to the conclusions drawn by Bonner and Nossal, who claim that dispersion in pathlength is not a large factor in a typical laser-Doppler application.[16]

In contrast, the spatial LDF perfusion fluctuations observed by e.g. Tenland *et al*[30] and Braverman *et al*[31], are most likely related to the underlying microvascular anatomy as well as temporal blood flow fluctuations, and not to local variations in the optical properties of the tissue, since we only found a 3-6% (CV) intra-site variability in $\widehat{pl}_i'$. Tenland *et al* presented LDF perfusion values from dorsal forearm skin in six adjacent sites, 2.5 mm apart, and from one site with the probe rotated 90 degrees between each measurement, corresponding to a 0.5 mm translation of the source fiber. According to our calculations, the average CVs of their LDF perfusion estimates were 37 and 16 %, respectively. Braverman *et al* indicated that a 100 % variation could be seen in the chest, back and abdominal skin LDF red blood cell flux, when moving the probe over distances of 2 - 6 mm. Correlations were found with the underlying vascular anatomy. The specific dimensions of the opical fibers are not clear in either paper, but surface sampling areas of 1 mm^2 are mentioned. We found an average CV of the LDF perfusion of about 17 % at a source detector separation of 1.15 mm ($Perf_{L5}$) in volar forearm skin, irrespective of whether the measurements were carried out repeatedly in the exact same location, or as a scan of five adjacent points, separated by one mm. This suggests that the intra-site LDF perfusion variations originate mainly from temporal variations rather than spatial variations in the true blood perfusion or optical properties, when using a fiber separation of ~1 mm. For comparison, Tenland *et al* reported on an 8 to 19 % CV of the LDF signal in one location on forearm skin, related to temporal blood flow variations over a 20-minute period.[30] Interestingly, $Perf_{L1}$ (fiber separation: 0.23 mm) varies up to 60 % more than $Perf_{L5}$ (fiber separation: 1.15 mm) when comparing the scans on fingertip (Table 4). One possible explanation is the high spatial resolution of the detector fiber closest to the source, i.e. the small sampling volume that the LDF perfusion signal is averaged over, rendering it more sensitive even to minor variations in the microvascular architecture.[31] Not only does a small source detector separation result in a small sampling volume, but also a superficial sampling depth. Larsson *et al* have shown that such a superficial sampling depth is associated with a significantly higher sensitivity to variations in optical properties, especially when measuring on a deep discrete blood flow.[21]

The predicted absorption coefficients, $\hat{\mu}_a$, displayed a tenfold greater estimation error than the corresponding reduced scattering coefficients, $\hat{\mu}_s'$, using the main reference and validation data set. By narrowing the μ_a-span of the reference set according to Table 1, the error of $\hat{\mu}_a$ was reduced a factor three, to 11%. The large errors in $\hat{\mu}_a$ are most likely due to the combination of small fiber separations, i.e. short pathlengths, and low μ_a values; hence, the absorption only has a minute influence on the diffuse reflectance profile. In addition, the span of μ_a in the simulation setup was up to a factor 60 greater than that of μ_s', rendering predictions of μ_a less precise. Adding noise to the simulated reflectance did reduce the precision of $\hat{\mu}_s'$; nevertheless, errors were not exceeding 7%,

which must be considered robust and satisfactory. However, the added noise produced further imprecision of $\hat{\mu}_a$, with errors up to 51 %. Improvement in the robustness of $\hat{\mu}_a$ was seen, if more detecting fibers with greater source detector separations were incorporated in the fitting of the diffuse reflectance profile to Equation 7. Similar improvement was observed when narrowing the range of μ_a in the reference set, or by excluding the lowest values of μ_a in the validation sets. This is in agreement with the results of other authors.[6,11] The imprecision of the *in vivo* estimated $\hat{\mu}_a$, might, for two reasons, be smaller than the imprecision presented above; a) most of the presented *in vivo* data (89%) were estimated using the joined sub reference set; b) the degree of added noise (rms of 5%) is probably overestimated since it was based on measurements on tissue phantom B which differ substantially from the expected *in vivo* optical properties. Therefore, the true imprecision of the presented *in vivo* $\hat{\mu}_a$ is more likely to be somewhere between 11% and 29% (sub reference set in Table 3).

In general, validation of a method using merely simulations or analytical modeling can be questioned. Therefore, we used tissue phantoms with well-defined optical properties to link simulations with measurements, and for method validation. The estimation error of the optical properties of the tissue phantom was about 12-15 % for the measurements, and 5-9 % for the simulations. Thus, the estimation error partly originates from the MPR algorithm *per se*, and partly from the link between the measurements and the simulations.

Estimation of the optical properties displayed an approximately fourfold increase (Table 4) in variation on going from measurements on one fixed site (arm_A, Figure 4), to a scan over five millimeters in an adjacent location (arm_B, Figure 4). This result clearly indicates that a great portion of the variations in measured optical properties was related to true local fluctuations in the tissue optical properties, and not merely due to prediction errors. Further, optical properties differ more comparing two different skin sites, e.g. fingertip and forearm, as opposed to multiple measurements in adjacent areas, such as $finger_A$ and $finger_B$ (Figure 4).

At λ = 632.8 nm, $\hat{\mu}_s'$ was found to be approximately ~2.1 mm^{-1} in volar forearm skin, and ~1.4 mm^{-1} on fingertips, whereas corresponding values for $\hat{\mu}_a$ were ~0.05 mm^{-1} and ~0.007 mm^{-1}, respectively. This massive difference in μ_a cannot merely be explained by the estimation errors of μ_a, but rather by the concentration of melanin, one of the most significant chromophores at this wavelength.[32] It is reasonable to assume, that the melanin content is greater in the forerarm skin than in the skin of the volar aspect of the fingertip. In comparison, Doornbos *et al*[33] found $\hat{\mu}_a$ = 0.017 mm^{-1} and $\hat{\mu}_s'$ = 0.91 on volar forearm skin at 633 nm, using a diffuse reflectance approach with a maximum fiber separation of 16.79 mm. Corresponding values for foot sole were $\hat{\mu}_a$ = 0.0072 mm^{-1} and $\hat{\mu}_s'$ = 1.12 mm^{-1}. The predicted optical properties in foot sole are in good agreement with the values we found on fingertip, where the pigmentation is believed to be similar. The disagreement in both the absorption and reduced scattering coefficient estimates, in the case of volar forearm skin, can be attributed to the more superficial probing in the present study. The highly absorbing and scattering superficial epidermis[26] will thus have a considerably greater impact on our measurements, compared to the results of Doornbos *et al*.

The reason for merely predicting μ_s', and not trying to resolve it into μ_s and g, is that it is only possible to do so if the detected photons have traveled less than one reduced mean

free path ($mfp' = (\mu_s' + \mu_a)^{-1}$).[5] With the present probe design and optical properties of human skin, detected photons will have traversed considerably greater distances than one mfp'.

Finally, applying the calibration, linearization and pl_i'-normalization algorithms, it was not only possible to compare perfusion readings from different individuals and/or skin locations, but also perfusion measured by different fibers. An example of this is shown in Figure 5, where $Perf_{NLi}$, measured on the volar side of the forearm, is presented for three individuals and five different emitting receiving fiber separations. The increase in $Perf_{NLi}$ with fiber separation can most likely be explained by the fact that the true tissue perfusion is believed to increase with skin depth, due to the larger sizes of deeper lying vessels.[34] Since an increased fiber separation will increase the sampling depth, more distant fibers will display higher $Perf_{NLi}$ values. Consequently, $Perf_{NLi}$ vs ρ_i could be considered an indicator of the depth distribution of the true blood perfusion. This is a promising approach to a crude depth discriminating LDF technique, and warrants further investigation.

5. Conclusions

We have proposed methods, based on diffuse reflectance and Monte Carlo simulations, for local determination of photon pathlength and optical properties. The accuracy of the methods was good (2-7%) for pathlength and reduced scattering but poor for absorption estimation. *In vivo* reduced scattering and absorption estimations in Caucasian skin was systematically lower in the fingertip than in the forearm skin (633 nm). *In vivo* pathlength estimations in Caucasian human skin displayed a maximum variation of ~35 %, between individuals in similar locations, and within individuals when comparing forearm skin with fingertip. The variations within the fingertip and forearm skin sites were 3-6%. This suggests that it is necessary to compensate for variations in optical properties when comparing LDF-readings from different individuals and/or skin site but not when comparing readings from the same skin site and individual. A unique relationship between the LDF perfusion estimate and photon pathlength has been established, and can hence be used to eliminate the influence of pathlength on the LDF perfusion estimate. Potentially, this enables intra- and inter-individual comparisons of LDF perfusion estimates in different organs.

Acknowledgements

This study was supported by the European Commission through the SMT4-CT97-2148 contract. Under this contract, a cooperation runs between the Universities of Twente and Groningen (the Netherlands), Linköping and Malmö (Sweden), Toulouse (France), the companies Perimed AB (Sweden), Moor Instruments and Oxford Optronix (UK), and the Institute of Biocybernetics and Biomedical Engineering in Warsaw (Poland). Financial support was also received from the Swedish National Board of Excellence for Non-Invasive Medical Measurements (NIMED), the Swedish Heart Lung Foundation (project number 200141208), the Royal Swedish Academy of Sciences and MedComp AB, Sweden. Finally, we would like to acknowledge Dr. Wiendelt Steenbergen, University of Twente, the Netherlands, for providing us with the tissue phantoms.

References

1. J. R. Mourant, T. Fuselier, J. Boyer, T. M. Johnson, and I. J. Bigio, "Predictions and measurements of scattering and absorption over broad wavelength ranges in tissue phantoms," Applied Optics **36**(4), 949-957 (1997).
2. W.-F. Cheong, "Summary of optical properties," in *Optical-Thermal Response of Laser-Irradiated Tissue*, A. J. Welch and M. J. C. van Gemert, ed. (Plenum Press, New York, 1995), pp. 275-303.
3. B. J. Tromberg, N. Shah, R. Lanning, A. Cerussi, J. Espinoza, T. Pham, L. Svaasand, and J. Butler, "Non-Invasive *In Vivo* Characterization of Breast Tumors Using Photon Migration Spectroscopy," Neoplasia **2**(1-2), 26-40 (2000).
4. F. Bevilacqua, D. Piguet, P. Marquet, J. D. Gross, B. J. Tromberg, and C. Depeursinge, "*In vivo* local determination of tissue optical properties: applications to human brain," Applied Optics **38**(22), 4939-4950 (1999).
5. F. Bevilacqua and C. Depeursinge, "Monte Carlo study of diffuse reflectance at source-detector separations close to one transport mean free path," Journal of the Optical Society of America A **16**(12), 2935-2945 (1999).
6. J. S. Dam, P. E. Andersen, T. Dalgaard, and P. E. Fabricius, "Determination of tissue optical properties from diffuse reflectance profiles by multivariate calibration," Applied Optics **37**(4), 772-778 (1998).
7. J. S. Dam, C. B. Pedersen, T. Dalgaard, P. E. Fabricius, A. Prakasa, and S. Andersson-Engels, "Fiber optic probe for non-invasive real-time determination of tissue optical properties at multiple wavelengths," Applied Optics **40**(7), 1155-1164 (2001).
8. R. A. J. Groenhuis, J. J. Ten Bosch, and H. A. Ferwerda, "Scattering and absorption of turbid materials determined from reflection measurements. 2: Measuring method and calibration," Applied Optics **22**(16), 2463-2467 (1983).
9. J. M. Schmitt, G. X. Zhou, E. C. Walker, and R. T. Wall, "Multilayer model of photon diffusion in skin," Journal of the Optical Society of America A **7**(11), 2141-2153 (1990).
10. B. C. Wilson and S. L. Jacques, "Optical reflectance and transmission of tissues: principles and applications," IEEE Journal of Quantum Electronics **26**(12), 2186-2199 (1990).
11. A. Kienle, L. Lilge, M. S. Patterson, R. Hibst, R. Steiner, and B. C. Wilson, "Spatially resolved absolute diffuse reflectance measurements for noninvasive determination of the optical scattering and absorption coefficients of biological tissue," Applied Optics **35**(13), 2304-2314 (1996).
12. T. J. Pfefer, L. S. Matchette, C. L. Bennett, J. A. Wilke, A. J. Durkin, and M. N. Ediger, "Determination of optical properties in highly attenuating media with an endoscope-compatible reflectance approach,". in *Optical Biopsy IV*, R. R. Alfano, eds., Proc. SPIE **4613,** 212-221 (2002).
13. G. E. Nilsson, T. Tenland, and P. Å. Öberg, "Evaluation of a laser Doppler flowmeter for measurement of tissue blood flow," IEEE Transactions on Biomedical Engineering **27**(10), 597-604 (1980).
14. G. E. Nilsson, M. Arildsson, and M. Linden, "Recent development in laser Doppler perfusion imaging for two-dimensional tissue blood flow mapping," in *Biomedical Optical Instrumentation and Laser-Assisted Biotechnology*, A. M. Verga Scheggi, S. Martellucci, A. N. Chester, and R. Pratesi, ed. (Kluwer Academic Publishers, Dordrecht, 1996), pp. 109-119.
15. G. Nilsson, A. Jakobsson, and K. Wårdell, "Tissue perfusion monitoring and imaging by coherent light scattering,". in *Bioptics: Optics in Biomedicine and Environmental Sciences*, O. D. Soares and A. V. Scheggi, eds., Proc. SPIE **1524,** 90-109 (1992).
16. R. F. Bonner and R. Nossal, "2. Principles of Laser-Doppler Flowmetry," in *Laser-Doppler Blood Flowmetry*, A. P. Shepherd and P. Å. Öberg, ed. (Kluwer Academic Press, Massachusetts, USA, 1990), pp. 17-45.
17. R. F. Bonner and R. Nossal, "Model for laser Doppler measurements of blood flow in tissue," Applied Optics **20**(12), 2097-2107 (1981).
18. G. E. Nilsson, "Signal processor for Laser Doppler Tissue Flowmeters," Medical & Biological Engineering & Computing **22**(4), 343-348 (1984).
19. H. Nilsson, M. Larsson, G. E. Nilsson, and T. Strömberg, "Photon pathlength determination based on spatially resolved diffuse reflectance," Journal of Biomedical Optics **7**(3), 478-85 (2002).
20. R. Nossal, R. F. Bonner, and G. H. Weiss, "Influence of path length on remote optical sensing of properties of biological tissue," Applied Optics **28**(12), 2238-2244 (1989).

21. M. Larsson, W. Steenbergen, and T. Strömberg, "Influence of Optical Properties and Fibre Separation on Laser Doppler Flowmetry," Journal of Biomedical Optics **7**(2), 236-43 (2001).
22. S. T. Flock, M. S. Patterson, B. C. Wilson, and D. R. Wyman, "Monte Carlo Modeling of Light Propagation in Highly Scattering Tissues - I: Model Predictions and Comparison with Diffusion Theory," IEEE Transactions on Biomedical Engineering **36**(12), 1162-1168 (1989).
23. W. M. Star, "Diffusion theory of light transport," in *Optical-thermal response of laser-irradiated tissue*, A. J. Welch and M. J. C. van Gemert, ed. (Plenum Press, New York, 1995), pp. 131-191.
24. F. F. M. de Mul, M. H. Koelink, M. L. Kok, P. J. Harmsma, J. Greve, R. Graaff, and J. G. Aarnoudse, "Laser Doppler velocimetry and Monte Carlo simulations on models for blood perfusion in tissue," Applied Optics **34**(28), 6595-6611 (1995).
25. L. G. Henyey and J. L. Greenstein, "Diffuse radiation in the galaxy," Astrophysics Journal **93**, 70-83 (1941).
26. V. V. Tuchin, "Optical Properties of Tissues with Strong (Multiple) Scattering," in *Tissue Optics: Light Scattering Methods and Instruments for Medical Diagnosis*ed. (SPIE Press, Bellingham, Washington, USA, 2000), pp. 13-33.
27. M. J. C. van Gemert, S. L. Jacques, H. J. C. M. Sterenborg, and W. M. Star, "Skin Optics," IEEE Transactions on Biomedical Engineering **36**(12), 1146-1154 (1989).
28. R. Graaff, A. C. M. Dassel, M. H. Koelink, F. F. M. de Mul, J. G. Aarnoudse, and W. G. Zijlstra, "Optical proerties of human dermis *in vitro* and *in vivo*," Applied Optics **32**(4), 435-447 (1993).
29. G. E. Nilsson, T. Tenland, and P. Å. Öberg, "A new instrument for continuous measurement of tissue blood flow by light beating spectroscopy," IEEE Transactions on Biomedical Engineering **27**(1), 12-19 (1980).
30. T. Tenland, E. G. Salerud, G. E. Nilsson, and P. Å. Öberg, "Spatial and temporal variations in human skin blood flow," International Journal of Microcirculation: Clinical and Experimental **2**(2), 81-90 (1983).
31. I. M. Braverman, A. Keh, and D. Goldminz, "Correlation of Laser Doppler Wave Patterns with Underlying Microvascular Anatomy," The Journal of Investigative Dermatology **95**(3), 283-286 (1990).
32. S. L. Jacques, "Skin Optics,". 1998, http://omlc.ogi.edu/news/jan98/skinoptics.html.
33. R. M. P. Doornbos, R. Lang, M. C. Aalders, F. W. Cross, and H. J. C. M. Sterenborg, "The determination of in vivo human tissue optical properties and absolute chromophore concentrations usings spatially resolved steady-state diffuse reflectance spectroscopy," Physics in Medicine and Biology **44**(4), 967-981 (1999).
34. I. M. Braverman, "The cutaneous microcirculation," J Investig Dermatol Symp Proc **5**(1), 3-9. (2000).